Inorganic Chemistry

including bioinorganic chemistry

June 16, 2014
Volume 53, Number 12
pubs.acs.org/IC

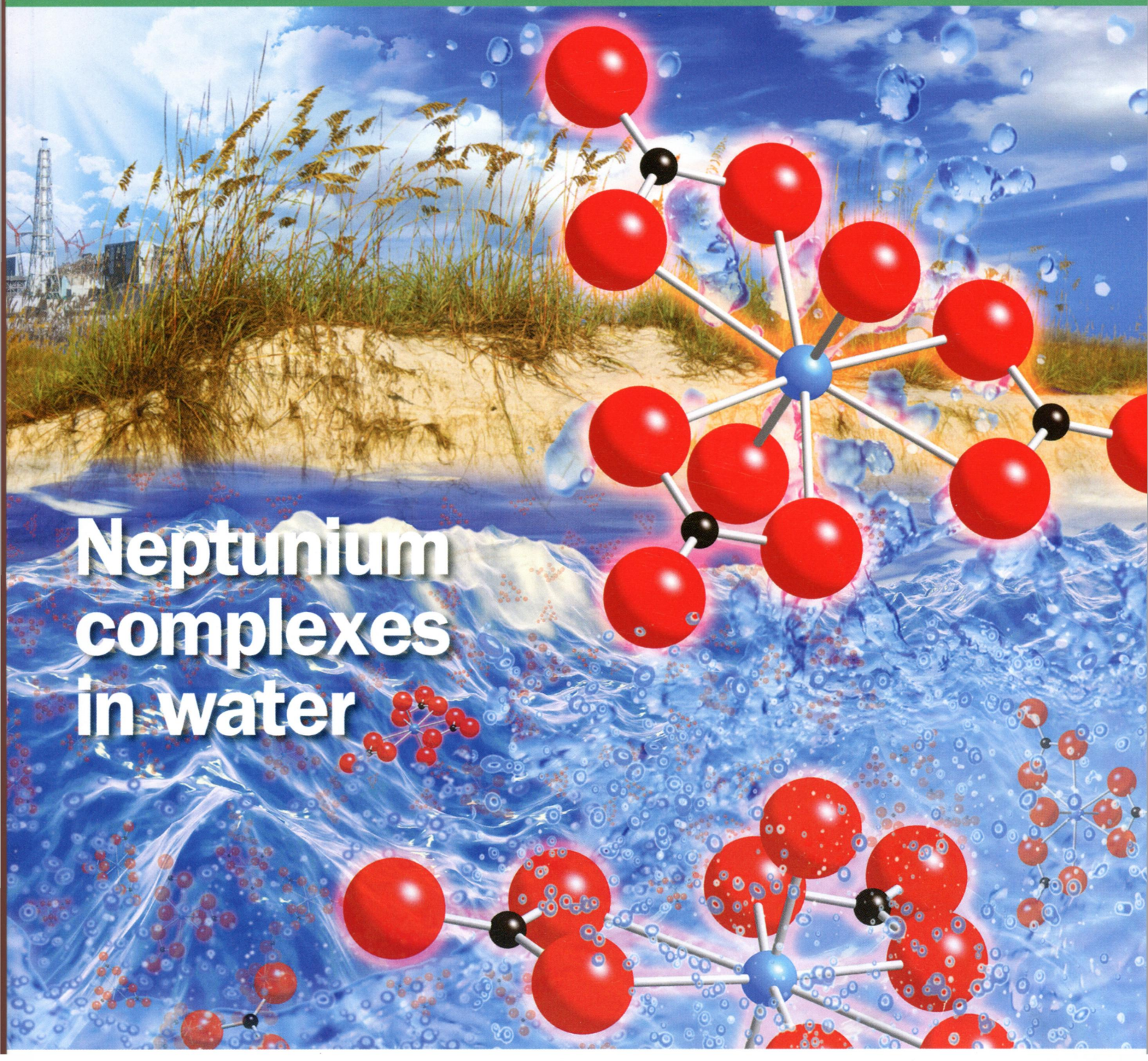

ACS Publications
Most Trusted. Most Cited. Most Read.

www.acs.org

Inorganic Chemistry

JUNE 16, 2014
VOLUME 53 ISSUE 12
INOCAJ 53(12) 5875–6356 (2014)
ISSN 0020-1669
Registered in the U.S. Patent and Trademark Office

ON THE COVER: The Np(VI)–tricarbonate ion is the most environmentally important Np(VI) species. On p 4208, Panasci, Harley, Zavarin, and Casey show that the carbonate ligand-exchange kinetics are quantitatively similar to those of the relatively benign U(VI)–tricarbonate ion. This paper was inadvertently published in a previous issue. See A. F. Panasci, S. J. Harley, M. Zavarin, and W. H. Casey *Inorg. Chem.* **2014**, *53* (8), 4202–4208.

Communications

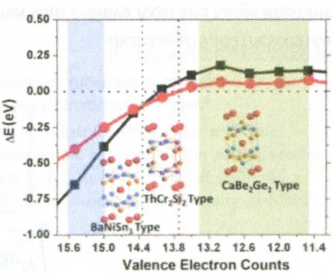

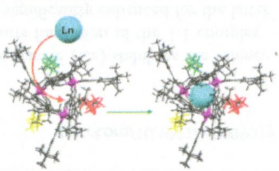

5881 S dx.doi.org/10.1021/ic500434a

Synthesis and Characterization of Metal–Organic Framework-74 Containing 2, 4, 6, 8, and 10 Different Metals

Lisa J. Wang, Hexiang Deng, Hiroyasu Furukawa, Felipe Gándara, Kyle E. Cordova, Dani Peri, and Omar M. Yaghi*

Metal–organic frameworks (MOFs) containing more than two types of metal ions mixed within one secondary building unit are rare because the synthesis often yields mixed MOF phases rather than a single, pure phase of a mixed-metal MOF. We used a one-pot solvothermal reaction to construct microcrystalline MOF-74 [M2(DOT); DOT = dioxidoterephthalate], which contains up to 10 (Mg, Ca, Sr, Ba, Mn, Fe, Co, Ni, Zn, and Cd) different kinds of metals.

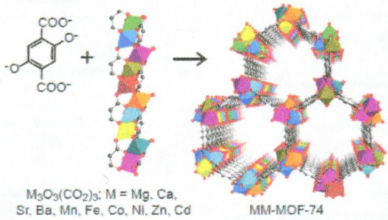

5884 S dx.doi.org/10.1021/ic5006727

Isomorphic Ti Substitution into SBA-15 without Ti Loss and with Lower TiO_2 Segregation

Jae Yul Kim, Jae Young Kim, Hyun Joon Kang, Won Yong Kim, Young Hye Lee, and Jae Sung Lee*

Ti atoms were incorporated into a SBA-15 lattice while keeping its mesoporous structure intact without Ti loss and with lower TiO_2 segregation by hydrolysis of a Ti precursor near neutral pH.

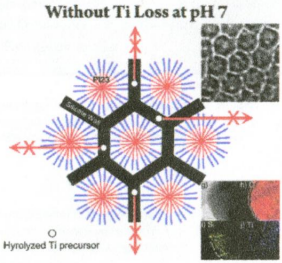

5887 S dx.doi.org/10.1021/ic500746e

Responsive Nature of 1,2,4,5-Tetrakis(2-pyridylthiomethyl)benzene Toward Group 12 Metal Nitrates: Activity of Coordinated Nitrate in Metal Complexes

Neeru, Dolly Yadav, Geeta Tiwari, Jai Deo Singh,* and Raymond J. Butcher

This study provides a detailed spectroscopic and X-ray crystallographic analysis on the responsive behavior of 1,2,4,5-tetrakis(2-pyridylthiomethyl)benzene (**L**) toward group 12 metal nitrates. These findings also provide some basic insight into the behavior of the nitrate ion, which plays a vital role in determining the dimensionality and structure of the coordination polymer.

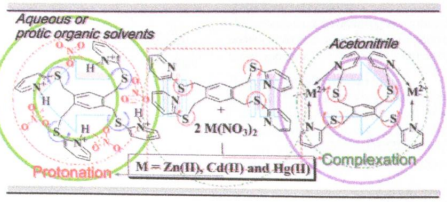

5890 dx.doi.org/10.1021/ic500820v

Isolable 1,1-Disubstituted Silole Dianion: a Homogeneous Two-Electron-Transfer Reducing Reagent

Zhengang Han, Jianfeng Li, Hongfan Hu, Jianying Zhang, and Chunming Cui*

The first isolable 1,1-disubstituted silole dianion **2** has been prepared and structurally characterized. The dianion underwent two-electron-transfer reactions with a variety of substrates to regenerate the corresponding silole. Reduction of $(Mes)_2SiCl_2$ with the dianion selectively yielded the cyclotrisilane $(Mes_2Si)_3$, demonstrating its potential use for the preparation of low-valent silicon species.

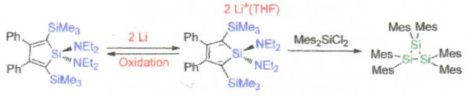

5893 dx.doi.org/10.1021/ic500901y

Activation of a High-Valent Manganese–Oxo Complex by a Nonmetallic Lewis Acid

Regina A. Baglia, Maximilian Dürr, Ivana Ivanović-Burmazović, and David P. Goldberg*

The addition of the nonmetal Lewis acid $B(C_6F_5)_3$ to a low-spin manganese(V)–oxo corrolazine (Cz) stabilizes the valence tautomer $Mn^{IV}(O)(Cz^{\bullet+})$. Cryospray mass spectrometry, together with other data, supports formation of the 1:1 complex $Mn^{IV}(O)(Cz^{\bullet+}):B(C_6F_5)_3$. The rates of hydrogen-atom abstraction from O–H bonds are significantly enhanced for the latter species. This work provides insight regarding the influence of both the electronic structure and Lewis acids on the reactivity of high-valent metal–oxo complexes.

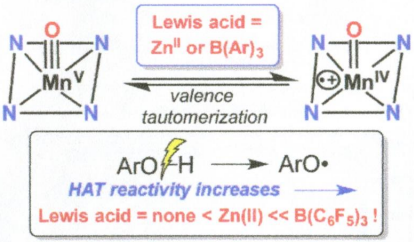

5896 dx.doi.org/10.1021/ic500916u

Slow Magnetic Relaxation in Octahedral Cobalt(II) Field-Induced Single-Ion Magnet with Positive Axial and Large Rhombic Anisotropy

Radovan Herchel, Lucia Váhovská, Ivan Potočňák, and Zdeněk Trávníček*

Pseudooctahedral mononuclear cobalt(II) complex $[Co(abpt)_2(tcm)_2]$ (**1**), where abpt = 4-amino-3,5-bis(2-pyridyl)-1,2,4-triazole and tcm = tricyanomethanide anion, shows field-induced slow relaxation of magnetization with $U = 86.2$ K and large axial and rhombic single-ion zero-field-splitting parameters, $D = +48(2)$ cm^{-1} and $E/D = 0.27(2)$ ($D = +53.7$ cm^{-1} and $E/D = 0.29$ from ab initio CASSCF/NEVPT2 calculations), thus presenting new example of a field-induced single-ion magnet with transversal magnetic anisotropy.

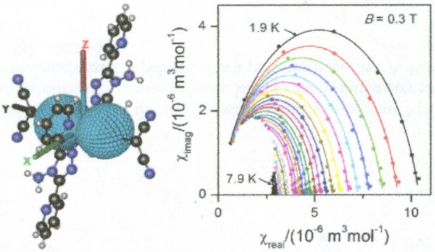

5899 Ⓢ dx.doi.org/10.1021/ic500964m

Cyanide-Bridged Decanuclear Cobalt–Iron Cage

Takuya Shiga, Tamaki Tetsuka, Kanae Sakai, Yoshihiro Sekine, Masayuki Nihei, Graham N. Newton, and Hiroki Oshio*

A decanuclear cobalt–iron cage complex, $(Et_4N)_2[Co(L^R)_2]_6[Fe(CN)_6]_4(BF_4)$, was obtained, and its magnetic properties and electronic configurations were investigated. Single-crystal X-ray and Mössbauer analyses showed the complex to display thermally controlled electron-transfer-coupled spin transition (ETCST) behavior between Co^{III} low-spin–NC–Fe^{II} low-spin and Co^{II} high-spin–NC–Fe^{III} low-spin states.

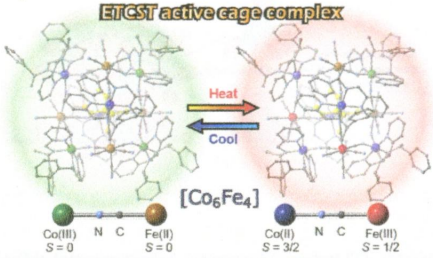

Articles

5902 Ⓢ dx.doi.org/10.1021/ic500627d

Tetranuclear Silver(I) Clusters Showing High Ionic Conductivity in a Bicontinuous Cubic Mesophase

Padi Y. S. Su, Jing C. W. Tseng, Kwang-Ming Lee, Ju-Chun Wang, and Ivan J. B. Lin*

Ionic metallomesogens composed of tetranuclear silver triazole complexes show the phase transition sequence of Cr → SmC → Cub → SmA → isotropic and exhibit superior ionic conductivity at a bicontinuous cubic mesophase because of the three-dimensional ion-transporting channels and the inherent lability of the Ag–N bond.

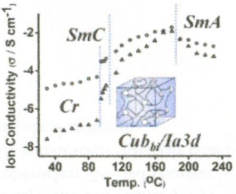

5911 Ⓢ dx.doi.org/10.1021/ic402988y

Crystallographic and Magnetic Structure of the Perovskite-Type Compound $BaFeO_{2.5}$: Unrivaled Complexity in Oxygen Vacancy Ordering

Oliver Clemens,* Melanie Gröting, Ralf Witte, J. Manuel Perez-Mato, Christoph Loho, Frank J. Berry, Robert Kruk, Kevin S. Knight, Adrian J. Wright, Horst Hahn, and Peter R. Slater

The crystal and magnetic structure of the vacancy-ordered perovskite-type compound $BaFeO_{2.5}$ has been solved. Mössbauer spectroscopy confirms the local coordination of the iron ions and the oxidation state of 3+. The G-type antiferromagnetic structure is in agreement with temperature-dependent measurements of the magnetic moment.

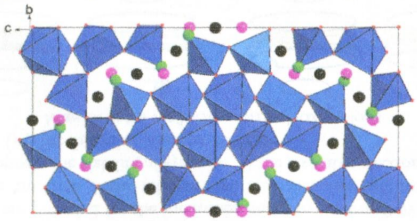

5922 S dx.doi.org/10.1021/ic403080n

Lanthanide Metalloligand Strategy toward d–f Heterometallic Metal–Organic Frameworks: Magnetism and Symmetric-Dependent Luminescent Properties

Xiao-feng Huang, Jing-xin Ma, and Wei-sheng Liu*

On the basis of lanthanide metalloligands, $[Ln(ODA)_3]^{3-}$ (H_2ODA = oxydiacetic acid), three series of d–f heterometallic metal–organic frameworks (HMOFs), $\{[Co(H_2O)_6]\cdot[Ln_2(ODA)_6Co_2]\cdot 6H_2O\}_n$ [**1**; Ln = Gd (**1a**), Dy (**1b**), and Er (**1c**)], $\{[Ln_2(ODA)_6Cd_3(H_2O)_6]\cdot nH_2O\}_n$ [**2**; Ln = Pr (**2a**), Nd (**2b**), Sm (**2c**), Eu (**2d**), and Dy (**2e**), n = 6 or 3], and $\{[Cd(H_2O)_6]\cdot[Ln_2(ODA)_6Cd_2]\cdot 6H_2O\}_n$ [**3**; Ln = Dy (**3a**), Ho (**3b**), Er (**3c**), Tm (**3d**), and Lu (**3e**), n = 6 or 12], were designed and synthesized by different synthesis methods. The results demonstrated that the lanthanide metalloligand strategy is an effective method to construct d–f HMOFs. The magnetism of **1** and luminescent properties of **2d** were also performed.

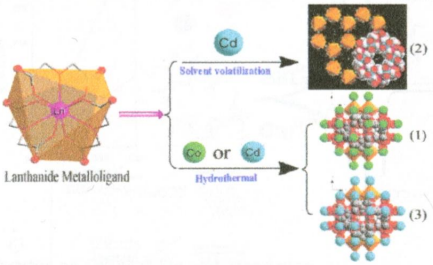

5931 S dx.doi.org/10.1021/ic500033b

Crystallographic and Spectroscopic Insights into Heme Degradation by *Mycobacterium tuberculosis* MhuD

Amanda B. Graves, Robert P. Morse, Alex Chao, Angelina Iniguez, Celia W. Goulding, and Matthew D. Liptak*

X-ray crystallography has revealed that *M. tuberculosis* MhuD stabilizes a ruffled heme substrate. ^{1}H nuclear magnetic resonance and variable temperature, variable field magnetic circular dichroism spectroscopic characterization of this species have demonstrated that MhuD stabilizes an unusual heme electronic structure with a $^2B_{2g}$ electronic ground state and a thermally accessible ^2E_g excited state. The data presented here strongly suggests that the α-meso regioselectivity of MhuD-catalyzed porphyrin cleavage depends on both structural and electronic factors.

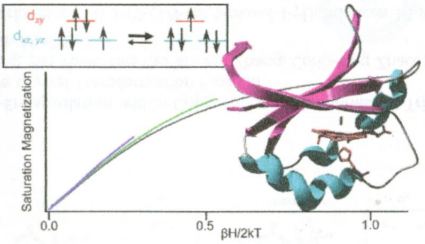

5941 S dx.doi.org/10.1021/ic500087t

Effect of Electron (De)localization and Pairing in the Electrochemistry of Polyoxometalates: Study of Wells–Dawson Molybdotungstophosphate Derivatives

Loïc Parent, Pablo A. Aparicio, Pedro de Oliveira, Anne-Lucie Teillout, Josep M. Poblet, Xavier López,* and Israël M. Mbomekallé*

Experimental and theoretical data are provided for the monosubstituted α_1- and α_2-$P_2W_{17}Mo$ anions and α-$P_2W_{18-x}Mo_x$ systems containing more than one Mo atom. Some relevant facts arise that may help to rationalize the redox behavior of POMs in general. Three aspects concern the stability of systems: (i) the favorable electron delocalization, (ii) the unfavorable $e^- - e^-$ electrostatic repulsion, and (iii) the favorable electron pairing.

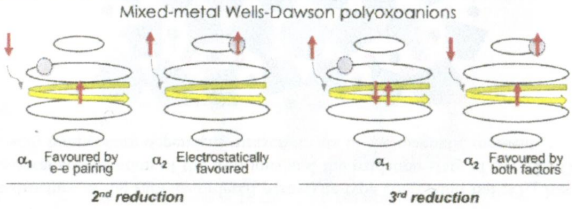

5950 S dx.doi.org/10.1021/ic500132n

Near-Infrared Luminescent PMMA-Supported Metallopolymers Based on Zn–Nd Schiff-Base Complexes

Zhao Zhang, Weixu Feng, Peiyang Su, Xingqiang Lü,* Jirong Song, Daidi Fan, Wai-Kwok Wong, Richard A. Jones, and Chengyong Su

The first example of Wolf Type II NIR luminescent Zn^{2+}–Nd^{3+}-containing metallopolymers **Poly(MMA-*co*-[Zn(L^n)(Py)-Nd(NO$_3$)$_3$])** is obtained from the controlled polymerization of MMA and two series of heterobinuclear Zn–Nd complexes **[Zn(L^n)(Py)Nd(NO$_3$)$_3$]** (n = 1 or 2), and the concentration self-quenching of Nd^{3+}-based NIR luminescent materials could be effectively prevented for the copolymerized hybrid materials in comparison with the doped hybrid materials.

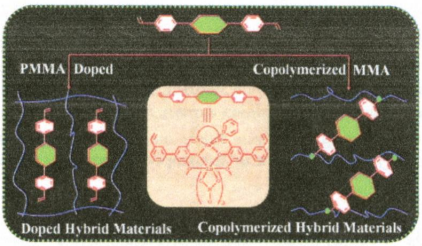

5961 dx.doi.org/10.1021/ic5001599

Synthesis, Structure, Luminescence, and Magnetic Properties of a Single-Ion Magnet *"mer"*-[Tris(*N*-[(imidazol-4-yl)-methylidene]-DL-phenylalaninato)terbium(III) and Related *"fac"*-DL-Alaninato Derivative

Suguru Yamauchi, Takeshi Fujinami, Naohide Matsumoto,* Naotaka Mochida, Takayuki Ishida,* Yukinari Sunatsuki, Masayuki Watanabe, Masanobu Tsuchimoto, Cecilia Coletti, and Nazzareno Re

Two Tb^{III} complexes exhibiting different coordination geometries *"fac"*-$[Tb^{III}(HL^{DL\text{-}ala})_3]\cdot 7H_2O$ and *"mer"*-$[Tb^{III}(HL^{DL\text{-}phe})_3]\cdot 7H_2O$ were synthesized. Magnetic data were analyzed by a spin Hamiltonian including the crystal field effect on the Tb^{III} ion. The resultant energy patterns indicate easy-axis and -plane anisotropies for *"mer"* and *"fac"* complexes, respectively. The *"mer"* complex showed an onset of out-of-phase alternating current magnetic susceptibility on cooling down to 1.9 K and magnetic hysteresis in the pulsed-field magnetization measurements below 1.6 K, but the *"fac"* complex did not. Both complexes showed efficient luminescence.

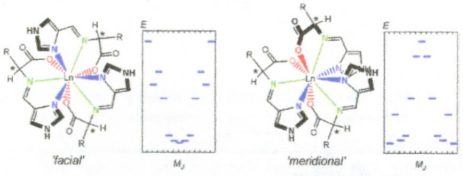

5972 dx.doi.org/10.1021/ic500183b

Anion-Exchange and Anthracene-Encapsulation within Copper(II) and Manganese(II)-Triazole Metal–Organic Confined Space in a Single Crystal-to-Single Crystal Transformation Fashion

Ju-Yan Liu, Qian Wang, Li-Jun Zhang, Bin Yuan, Yao-Yao Xu, Xin Zhang, Cong-Ying Zhao, Dan Wang, Yue Yuan, Ying Wang,* Bin Ding,* Xiao-Jun Zhao,* and Min Min Yue

Three novel coordination frameworks based on 1-(9-(1*H*-1,2,4-triazol-1-yl)anthracen-10-yl)-1*H*-1,2,4-triazole were isolated. Anion- and solvent-exchange experiments for **1** and **2** were determined in a single crystal-to-single crystal transformation fashion. Interestingly, when **3** was immersed in anthracene, light yellow crystals of **3** were dissolved and reassembled into dark brown crystals of **3a** with a 2D layer structure. Luminescent measurements indicate that **3a** is the first report of multidimensional polymers based on triazole derivatives as luminescent probes of Mg^{2+}.

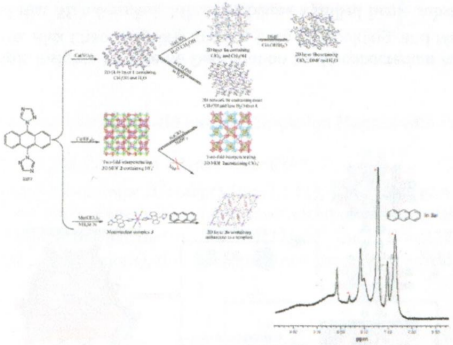

5986 dx.doi.org/10.1021/ic5002013

Chemical Composition, Crystal Structure, and Their Relationships with the Intrinsic Properties of Spinel-Type Crystals Based on Bond Valences

Xiao Liu, Hao Wang,* Barbara Lavina, Bingtian Tu, Weimin Wang, and Zhengyi Fu

The intrinsic properties, namely, compressibility and thermal expansion of spinel-type crystals, are closely related to the properties of chemical bonds in tetrahedral and octahedral coordination polyhedra. The coupled effects of the tetrahedral and octahedral frameworks on these intrinsic properties should be considered.

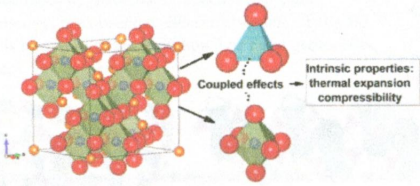

5993 dx.doi.org/10.1021/ic500234r

Stoichiometry-Controlled Two Flexible Interpenetrated Frameworks: Higher CO_2 Uptake in a Nanoscale Counterpart Supported by Accelerated Adsorption Kinetics

Nivedita Sikdar, Arpan Hazra, and Tapas Kumar Maji*

Two new interpenetrated 3D frameworks have been synthesized with different network topologies from the same set of organic linkers. One is further downsized to nanospheres through a coordination modulation method. On modulation, the nanosphere shows significantly enhanced CO_2 uptake properties due to higher mass diffusion into the framework at the nanoscale compared to bulk **1** under experimental conditions due to a lesser diffusion barrier. Water vapor adsorption studies further show that the rate of mass diffusion is significantly higher on the nanoscale compared to bulk.

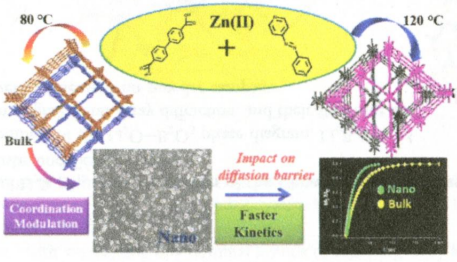

6003 S

dx.doi.org/10.1021/ic500244p

Aqueous Complexes for Efficient Size-based Separation of Americium from Curium

Mark P. Jensen,* Renato Chiarizia, Ilya A. Shkrob, Joseph S. Ulicki, Brian D. Spindler, Daniel J. Murphy, Mahmun Hossain, Adrián Roca-Sabio, Carlos Platas-Iglesias, Andrés de Blas, and Teresa Rodríguez-Blas*

The actinide ions americium(III) and curium(III) are difficult to separate from each other because they are close in size and are difficult to oxidize. The ligand *N,N'*-bis[(6-carboxy-2-pyridyl)methyl]-1,10-diaza-18-crown-6 (H_2bp18c6) both binds the larger Am^{III} ion more strongly than the Cm^{III} ion, reversing the usual order of complex stability, and favors complexation of actinide(III) ions over similarly sized lanthanide(III) ions. The Am/Cm selectivity of $bp18c6^{2-}$, 4.1, is the largest reported so far for binary An^{III}–ligand complexes.

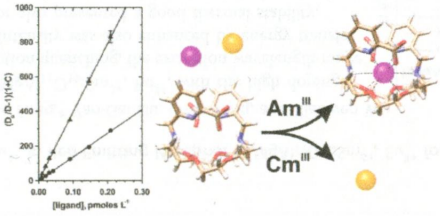

6013 S

dx.doi.org/10.1021/ic500282n

Effect of Lanthanide Complex Structure on Cell Viability and Association

Katie L. Peterson, Jonathan V. Dang, Evan A. Weitz, Cutler Lewandowski, and Valérie C. Pierre*

The effects of hydrophobicity and complex charge on cell viability and association are evaluated in a systematic study. Even the most lipophilic macrocyclic polyaminocarboxyalamide complexes exhibit low cellular association.

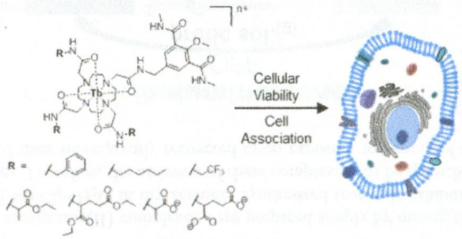

6022 dx.doi.org/10.1021/ic5003012

Substituent Effects on Spin State in a Series of Mononuclear Manganese(III) Complexes with Hexadentate Schiff-Base Ligands

Brendan Gildea, Michelle M. Harris, Laurence C. Gavin, Caroline A. Murray, Yannick Ortin, Helge Müller-Bunz, Charles J. Harding, Yanhua Lan, Annie K. Powell, and Grace G. Morgan*

Spin state choice in two series of cationic mononuclear manganese(III) complexes with a pair of closely related hexadentate ligands and five common anions is examined in solution and the solid state. Several of the complexes show a rare solid-state spin crossover, and the anion is found to be the more dominant determinant of spin state. A systematic increase in $T_{1/2}$ was observed on increasing the size of the ligand substituent from methoxy to ethoxy.

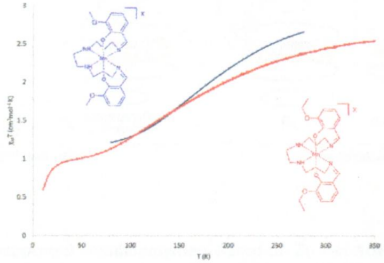

6034 dx.doi.org/10.1021/ic500331u

Crystal Structures of $Li_6B_4O_9$ and $Li_3B_{11}O_{18}$ and Application of the Dimensional Reduction Formalism to Lithium Borates

Gwenaëlle Rousse,* Benoît Baptiste, and Gérald Lelong*

The crystal structures of two members of the $Li_2O-B_2O_3$ phase diagram, $Li_6B_4O_9$ and $Li_3B_{11}O_{18}$, have been solved from single-crystal X-ray diffraction, and their structure has been further confirmed by Rietveld refinement on powder samples.

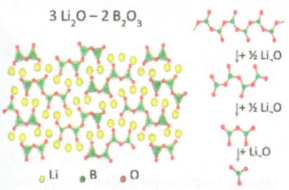

6042 dx.doi.org/10.1021/ic500356b

Heterometallic 3d–4f Coordination Polymers Based on 1,4,7-Triazacyclononane-1,4,7-triyl-tris(methylenephosphonate)

Yan-Hui Su, Song-Song Bao, and Li-Min Zheng*

On the basis of 1,4,7-triazacyclononane-1,4,7-triyl-tris(methylenephosphonic acid) (notpH6), layer compounds [FeLn-(notpH)(H2O)4]ClO4·5H2O [Ln = Nd (**FeNd**), Gd (**FeGd**), Sm (**FeSm**), Eu (**FeEu**)] and chain compound [CuLa(notpH2)(H2O)2]ClO4·3H2O (**CuLa**) are reported.

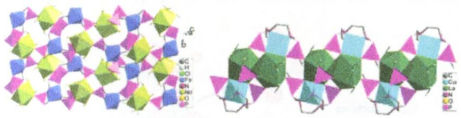

6048 Ⓢ dx.doi.org/10.1021/ic500381z

Local Structure and La L_1 and L_3-Edge XANES Spectra of Lanthanum Complex Oxides

Hiroyuki Asakura, Tetsuya Shishido,* Kentaro Teramura, and Tsunehiro Tanaka*

La L_1 and L_3-edge X-ray absorption near edge structure of various La oxides were classified according to local structure of La. We found a correlation between both of the areas of the pre-edge peaks of these spectra, the full width at half-maximum of white line of these spectra, and the local configuration of La. Simplified bond angle analysis is proposed to aid quantitative analysis of these spectra and the local configuration of La materials.

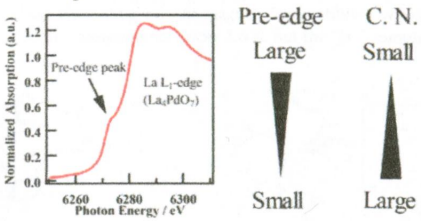

6054 Ⓢ dx.doi.org/10.1021/ic500400y

Triboluminescence and Vapor-Induced Phase Transitions in the Solids of Methyltriphenylphosphonium Tetrahalomanganate(II) Complexes

Sujitha Balsamy, Palani Natarajan,* Rathinavel Vedalakshmi, and Srinivasan Muralidharan

Novel triboluminescence active manganese(II) complexes were prepared simply by mixing the methyltriphenylphosphonium bromide with $MnBr_2{\cdot}4H_2O$ and $MnCl_2{\cdot}4H_2O$ in dry acetone. Synthesized materials exhibited phase transition character depending upon the surroundings. Therefore, the emission of these complexes can be quenched by exposing the complexes to vapors of the protic solvents and then subsequently recovered upon exposure to vapors of the aprotic solvents for multiple times.

6060 dx.doi.org/10.1021/ic500412r

Energy Transfer from Sm^{3+} to Eu^{3+} in Red-Emitting Phosphor $LaMgAl_{11}O_{19}:Sm^{3+}$, Eu^{3+} for Solar Cells and Near-Ultraviolet White Light-Emitting Diodes

Xin Min, Zhaohui Huang, Minghao Fang,* Yan-Gai Liu, Chao Tang, and Xiaowen Wu

In the red-emitting phosphor $LaMgAl_{11}O_{19}:Sm^{3+}$, Eu^{3+}, with the high doping content of Eu^{3+} without concentration quenching, the excitation wavelength range was extended, and the emission intensity was also enhanced by energy transfer from Sm^{3+} to Eu^{3+}. The phosphor also presented a good thermal stability. $LaMgAl_{11}O_{19}:0.05Sm^{3+}$, $0.2Eu^{3+}$ phosphor is a candidate for CuPc-based solar cells and white light-emitting diodes.

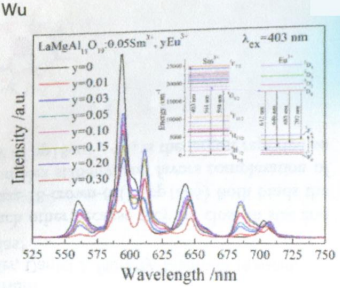

6066 S dx.doi.org/10.1021/ic5004275

Flexible Binding of PNP Pincer Ligands to Monomeric Iron Complexes

Kathlyn L. Fillman, Elizabeth A. Bielinski, Timothy J. Schmeier, Jared C. Nesvet, Tessa M. Woodruff, Cassie J. Pan, Michael K. Takase, Nilay Hazari,* and Michael L. Neidig*

The syntheses of the five-coordinate Fe(II) complexes, (^{R}PNP)FeCl$_2$ (^{R}PNP = HN{CH$_2$CH$_2$(PR$_2$)}$_2$, R = *i*Pr, *t*Bu, or cyclohexyl) are reported. Using a combination of techniques, including X-ray crystallography, Mössbauer spectroscopy, and magnetic circular dichroism spectroscopy, we observed different isomers of the Fe complexes, where the pincer ligand is bound in either meridional or facial geometries, both in solution and the solid state.

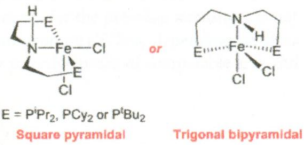

6073 S dx.doi.org/10.1021/ic500445b

Isolation of a Hexanuclear Chromium Cluster with a Tetrahedral Hydridic Core and Its Catalytic Behavior for Ethylene Oligomerization

Ahmed Alzamly, Sandro Gambarotta,* Ilia Korobkov, Muralee Murugesu, Jennifer J. H. Le Roy, and Peter H.M. Budzelaar*

A hexanuclear chromium cluster with a tetranuclear hidridic core and two peripheral chromium atoms has been obtained upon treatment of a trivalent precursor with aluminum alkyls.

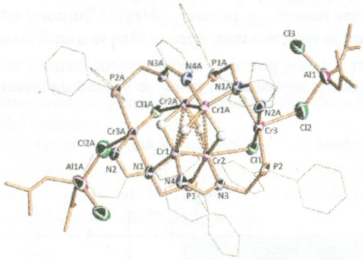

6082 S dx.doi.org/10.1021/ic500452h

Sensitivity of the Valence Structure in Diruthenium Complexes As a Function of Terminal and Bridging Ligands

Abhishek Mandal, Hemlata Agarwala, Ritwika Ray, Sebastian Plebst, Shaikh M. Mobin, José Luis Priego, Reyes Jiménez-Aparicio,* Wolfgang Kaim,* and Goutam Kumar Lahiri*

Interchanging the σ-donating acac$^-$ with π-accepting bpy terminal ligands or replacing O by less electronegative NH donor atoms in the 1,4-disubstituted 9,10-anthraquinone bridge affects the valence distribution between metals and bridge of corresponding diruthenium complexes in a subtle but reproducible way.

6094 dx.doi.org/10.1021/ic5004676

Significant Influence of Coligands Toward Varying Coordination Modes of 2,2′-Bipyridine-3,3′-diol in Ruthenium Complexes

Prabir Ghosh, Prasenjit Mondal, Ritwika Ray, Ankita Das, Sukdev Bag, Shaikh M. Mobin, and Goutam Kumar Lahiri*

The strongly π-accepting phenylazopyridine in **2** facilitates the stabilization of the O^-,O^- bonded seven-membered chelate involving deprotonated and twisted 2,2′-bipyridine-3,3′-diol.

2

6107 dx.doi.org/10.1021/ic5004879

Novel Isopolyoxotungstate $[H_2W_{11}O_{38}]^{8-}$ Based Metal Organic Framework: As Lewis Acid Catalyst for Cyanosilylation of Aromatic Aldehydes

Qiuxia Han,* Xueping Sun, Jie Li, Pengtao Ma, and Jingyang Niu*

A novel polyoxometalate-based metal organic framework constructed from an isolated isopolyoxotungstate $[H_2W_{11}O_{38}]^{8-}$ cluster is first synthesized by precursor $[W_{10}O_{32}]^{4-}$ under solvothermal conditions, which can act as Lewis acid catalyst to prompt the cyanosilylation with excellent efficiency in a heterogeneous manner.

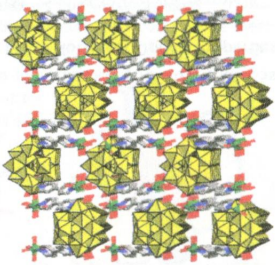

6113 dx.doi.org/10.1021/ic5005215

New Water-Soluble Ruthenium(II) Terpyridine Complexes for Anticancer Activity: Synthesis, Characterization, Activation Kinetics, and Interaction with Guanine Derivatives

Ana Rilak, Ioannis Bratsos,* Ennio Zangrando, Jakob Kljun, Iztok Turel, Živadin D. Bugarčić, and Enzo Alessio*

A series of new, water-soluble, monofunctional ruthenium(II) complexes with meridional geometry of the general formula *mer*-$[Ru(L_3)(N\text{-}N)X][Y]_n$ (where L_3 = Cl-tpy or tpy; N-N = en, dach, or bpy; X = Cl or dmso-*S*; Y = Cl, PF_6, or CF_3SO_3; n = 1 or 2, depending on the nature of X) were synthesized and fully characterized. The chlorido derivatives proved to be labile in aqueous solution and capable of interacting with guanine derivatives, whereas the dmso derivatives are inert. Overall, the complexes with bidentate aliphatic diamines proved to be superior to those with bpy in terms of solubility and reactivity.

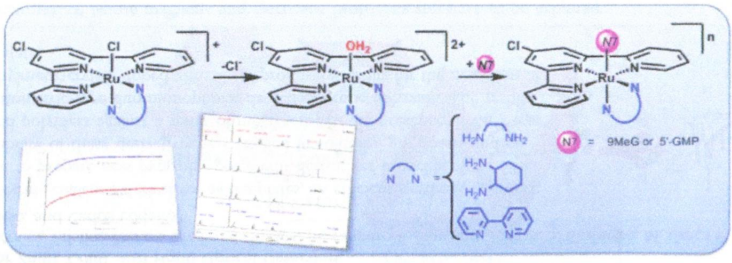

6127 dx.doi.org/10.1021/ic500528f

Effect of Cobalt Substitution on $Li_{3-2x}Co_xN$ Local Structure: A XAS Investigation

Diane Muller-Bouvet,* Jean-Pierre Pereira-Ramos, Stéphane Bach, Patrick Willmann, and Alain Michalowicz

The Co−N bond length in $Li_{3-2x}Co_xN$ compounds is obtained vs x by performing EXAFS fitting and found to be shorter (1.80 Å) than for $x = 0$ (Li_3N), and its value does not change with x. We show that the continuous decrease of interlayer distance versus Co content (x), described from XRD data, accounts for an average of the Co−N and Li−N distances, weighted by the number of these bond lengths.

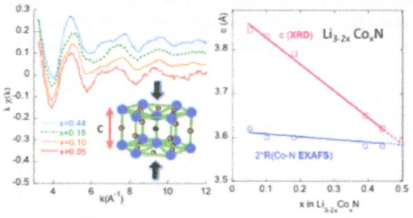

6132 dx.doi.org/10.1021/ic500536h

Oxaphosphirane-Borane Complexes: Ring Strain and Migratory Insertion/Ring-Opening Reactions

Arturo Espinosa,* Edgar de las Heras, and Rainer Streubel*

Increased ring strain of the oxaphosphirane ring and enhanced electron density at B is observed due to effective charge transfer upon *P*-complexation with BR_3; as a consequence migratory insertion/ring-opening reactions of groups R to ring atom positions are promoted.

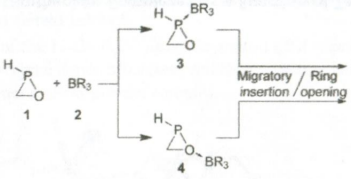

6141 dx.doi.org/10.1021/ic5005984

Synthesis, Crystal Structure, and Magnetic Properties of Novel Intermetallic Compounds R_2Co_2SiC (R = Pr, Nd)

Sixuan Zhou, Trinath Mishra, Man Wang, Michael Shatruk, Huibo Cao, and Susan E. Latturner*

R_2Co_2SiC (R = Pr, Nd) intermetallics were grown as large crystals from reactions of carbon and silicon in R/Co eutectic melts. These phases have a new structure type featuring puckered layers of R^{3+} cations sandwiched between Co/Si/C sheets. Magnetic susceptibility studies, single-crystal neutron diffraction data, and DOS calculations indicate the cobalt has a negligible magnetic moment, and the R^{3+} cations order ferromagnetically in both analogues.

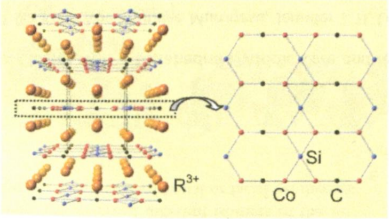

6149 Ⓢ dx.doi.org/10.1021/ic500634y

Synthesis, Spectroscopy Studies, and Theoretical Calculations of New Fluorescent Probes Based on Pyrazole Containing Porphyrins for Zn(II), Cd(II), and Hg(II) Optical Detection

Nuno M. M. Moura, Cristina Núñez, Sérgio M. Santos, M. Amparo F. Faustino, José A. S. Cavaleiro, M. Graça P. M. S. Neves,* José Luis Capelo, and Carlos Lodeiro*

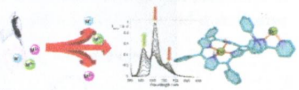

Using β-porphyrin–chalcone derivatives as templates, an efficient synthetic approach was developed to prepare new pyrazole–porphyrin derivatives in yields up to 82%. The sensing ability of these derivatives was studied in solution, gas phase, and on solid-supported polymers against a series of metal ions. In the presence of Zn^{2+} was observed a ratiometric-type fluoroionophoric detection probe behavior. The results with polymethylmethacrylate doped films show promising results for the detection of Zn^{2+} in solid state.

6159 Ⓢ dx.doi.org/10.1021/ic5006693

Redox Chemistry of Nickel(II) Complexes Supported by a Series of Noninnocent β-Diketiminate Ligands

June Takaichi, Yuma Morimoto, Kei Ohkubo, Chizu Shimokawa, Takayuki Hojo, Seiji Mori,* Haruyasu Asahara, Hideki Sugimoto, Nobutaka Fujieda, Nagatoshi Nishiwaki, Shunichi Fukuzumi, and Shinobu Itoh*

Nickel complexes of a series of β-diketiminate ligands (deprotonated form of 2-substituted *N*-[3-(phenylamino)allylidene]-aniline derivatives, $^{R}L^{-}$, R = Me, H, Br, CN, and NO_2) have been synthesized and structurally characterized. One-electron oxidation of the neutral complexes $[Ni^{II}(^{R}L^{-})_2]$ gave the corresponding cationic complexes, $[Ni^{II}(^{R}L^{0.5\bullet-})_2]^+$, in which β-diketiminate was oxidized acting as a noninnocent ligand, and the generated radical spin equally delocalizes into the two ligands giving class III mixed-valence speceis, whereas one-electron reduction took place at the metal center to give the anionic nickel(I) complexes $[Ni^{I}(^{R}L^{-})_2]^-$. Substituent effects on the electronic structures of the three oxidation states (neutral, cationic, and anionic) of the complexes are systematically evaluated using DFT calculations.

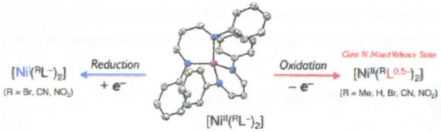

6170 Ⓢ dx.doi.org/10.1021/ic500655s

On the Potential Application of Superalkali Clusters in Designing Novel Alkalides with Large Nonlinear Optical Properties

Wei-Ming Sun, Li-Tao Fan, Ying Li, Jia-Yuan Liu, Di Wu,* and Zhi-Ru Li

A new series of superalkali-based alkalides Li_3^+(calix[4]pyrrole)M^-, Li_3O^+(calix[4]pyrrole)M^-, and M_3O^+(calix[4]pyrrole)K^- (M = Li, Na, and K) have been designed and systemically studied by the density functional theory method. These species have diverse structural isomers, in which the embedded superalkalis maintain their identities. Besides, all the investigated alkalides show large NLO responses, especially for the potassides.

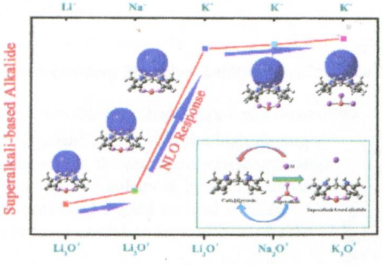

6179 S

dx.doi.org/10.1021/ic5006902

Mn K-Edge X-ray Absorption Studies of Oxo- and Hydroxo-manganese(IV) Complexes: Experimental and Theoretical Insights into Pre-Edge Properties

Domenick F. Leto and Timothy A. Jackson*

Experimental and theoretical studies were performed to correlate the Mn pre-K-edge data for Mn^{IV}=O and Mn^{IV}–OH adducts with geometric and electronic structure. Mn 3d-4p mixing, which primarily accounts for the pre-edge intensities, is not solely a function of the Mn–O(H) bond length but is modulated by the coordination geometry. Thus, depending on the specifics of the ligand field, Mn^{IV}–OH, Mn^{IV}=O, and even Mn^{V}=O species can show pre-edge peaks of comparable area and height.

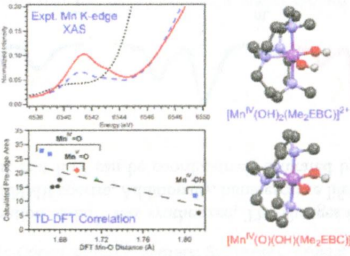

6195 S

dx.doi.org/10.1021/ic500682t

Synthesis and Structural Studies of Diorganotin(IV)-Based Coordination Polymers Bearing Silaalkylphosphonate Ligands and Their Transformation into Colloidal Domains

Ravi Shankar,* Nisha Singla, Meenal Asija, Gabriele Kociok-Köhn, and Kieran C. Molloy

Synthesis and structural studies of silaalkylphosphonic acids $Me_3SiCR_2P(O)(OH)_2$ (R = H, CH_3) and diorganotin-based coordination polymers derived therefrom are described. The formation of colloidal particles of $Et_2Sn(O_3PCH_2SiMe_3)$ featuring rodlike morphology was achieved by a wet chemical approach.

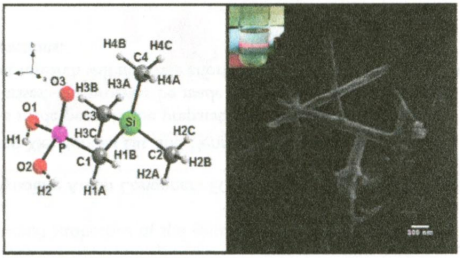

6204 dx.doi.org/10.1021/ic5007007

Luminescence Modulations of Rhenium Tricarbonyl Complexes Induced by Structural Variations

Hélène C. Bertrand,* Sylvain Clède, Régis Guillot, François Lambert, and Clotilde Policar

Re(I) tricarbonyl complexes are of considerable interest as bioimaging probes. Single-core multimodal probes for imaging (SCoMPIs) display unique photophysical properties enabling their unequivocal detection in cells. New SCoMPIs were prepared from an ancillary 1-(2-pyridyl)-1,2,3-triazole ligand, denoted Tapy, a regioisomer of the widely used Pyta ligand. When functionalized with long alkyl chains, they show impressive enhancement of their luminescent properties relative to the parent Pyta complex, both in solution and in MDA-MB231 breast cancer cells.

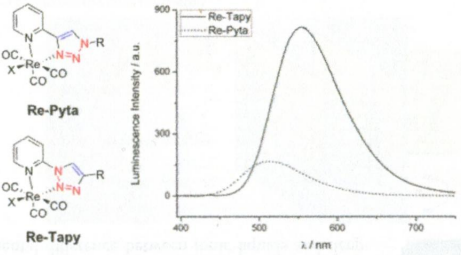

6224 dx.doi.org/10.1021/ic500740r

Supramolecular Control of a Mononuclear Biomimetic Copper(II) Center: Bowl Complexes vs Funnel Complexes

Jérôme Gout, Aleksandar Višnjevac,* Stéphanie Rat, Arnaud Parrot, Assia Hessani, Olivia Bistri, Nicolas Le Poul, Yves Le Mest, and Olivia Reinaud*

The resorcinarene-based tris-imidazole ligand allows supramolecular control of a Cu^{II} ion in a biomimetic environment. An XRD structure shows a square-based pyramidal environment for Cu^{II} with an acetate ligand deeply included in the bowl-shaped macrocycle. Solution studies of the coordination properties of the metal center and redox behavior of the associated Cu^{II}/Cu^{I} couple together with a comparison with the related funnel complexes further highlight the importance of the cavity providing a well-defined first, second, and third coordination sphere.

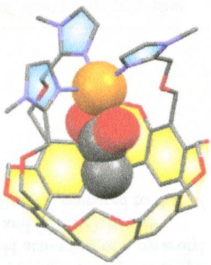

6235 dx.doi.org/10.1021/ic5007567

Framework Structures of Interconnected Layers in Calcium Iron Arsenides

Tobias Stürzer, Christine Hieke, Catrin Löhnert, Fabian Nitsche, Juliane Stahl, Christian Maak, Roman Pobel, and Dirk Johrendt*

New iron arsenide materials with so far unknown crystal structures demonstrate a remarkable structural flexibility of this class of compounds beyond the simple layered structures well-known from iron-based high-T_c superconductors. In the new compounds, iron arsenide tetrahedral layers are bridged through like fragments, giving rise to structures with new frameworks of interconnected layers, whose magnetic and electronic properties still have to be explored.

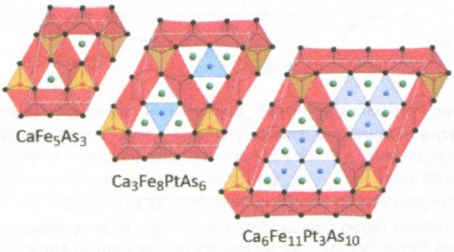

6241 S

dx.doi.org/10.1021/ic500778n

Role of Acentric Displacements on the Crystal Structure and Second-Harmonic Generating Properties of $RbPbCO_3F$ and $CsPbCO_3F$

T. Thao Tran, P. Shiv Halasyamani,* and James M. Rondinelli*

Two lead fluorocarbonates, $RbPbCO_3F$ and $CsPbCO_3F$, were synthesized and characterized. Both materials exhibit three-dimensional structures consisting of corner-sharing $Pb(CO_3)_3F_2$ polyhedra. The bridging F atom in $RbPbCO_3F$ is statistically disordered in the *ab*-plane, whereas that in $CsPbCO_3F$ is clearly disordered along the *c*-axis. $RbPbCO_3F$ and $CsPbCO_3F$ are noncentrosymmetric and crystallize in the achiral and nonpolar space group $P\bar{6}m2$. Additionally, an improved structural understanding of the acentric properties was developed through the specific acentric-mode displacements analyses.

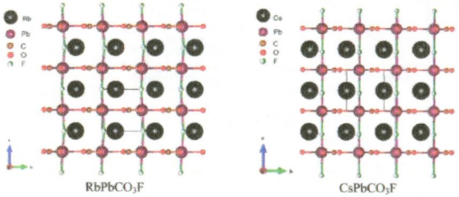

6252

dx.doi.org/10.1021/ic500780h

The Cyanate and 2-Phosphaethynolate Anion Congeners ECO^- (E = N, P, As, Sb, Bi): Prelude to Experimental Characterization

Yunxiang Lu,* Hui Wang, Yaoming Xie, Honglai Liu, and Henry F. Schaefer*

Pioneering synthetic research has made possible the preparation of 2-phosphaethynolates (PCO^-). The obvious question arises: can progress be made toward $AsCO^-$, $SbCO^-$, and $BiCO^-$? We hope that the present research will motivate efforts to prepare $SbCO^-$ and $BiCO^-$ in the laboratory and study their reactions.

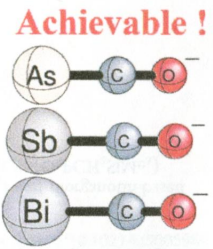

6257 S

dx.doi.org/10.1021/ic500790q

Synthesis, Spectroscopic Characterization, and Reactivity of Water-Tolerant Eu^{3+}-Based Precatalysts

Derek J. Averill and Matthew J. Allen*

A new set of chiral ligands for complexation of Eu^{3+} was synthesized. The changes in Eu^{3+} coordination environment were monitored using Eu^{3+} luminescence and NMR spectra. Additionally, luminescence lifetimes were used to monitor Eu^{3+}–water coordination numbers. The data suggest that Eu^{3+} can be coordinatively saturated by more than one hexadentate ligand to influence catalytic activity.

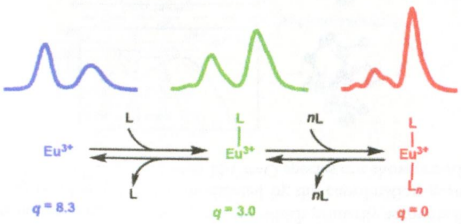

6264 dx.doi.org/10.1021/ic500803h

A Synthesis and Crystal Chemical Study of the Fast Ion Conductor $Li_{7-3x}Ga_xLa_3Zr_2O_{12}$ with $x = 0.08$ to 0.84

Daniel Rettenwander,* Charles A. Geiger, Martina Tribus, Peter Tropper, and Georg Amthauer

Fast-conducting cubic Ga-bearing $Li_7La_3Zr_2O_{12}$ (LLZO) has been synthesized using solid-state methods with 0.08 to 0.52 Ga^{3+} pfu in the garnet. An upper limit of 0.72 Ga^{3+} pfu in the garnet was obtained, but the synthesis product contained small amounts of $La_2Zr_2O_{12}$ and $LiGaO_3$. The NMR spectra are interpreted as indicating that Ga^{3+} mainly occurs in a distorted 4-fold coordinated environment that corresponds to the "non-standard" general *96h* crystallographic site.

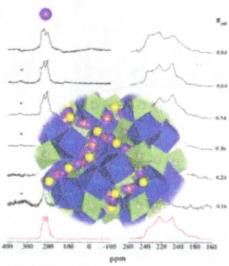

6270 dx.doi.org/10.1021/ic500811n

C–H Activation of Pyrazolyl Ligands by Ru(II)

Evan E. Joslin, Brandon Quillian, T. Brent Gunnoe,* Thomas R. Cundari,* Michal Sabat, and William H. Myers

$TpRu(P(OCH_2)_3CEt)(NCMe)Ph$ is effective for intermolecular activation of aromatic C–H bonds and catalytic olefin hydroarylation. In contrast, upon heating, the cationic Ru(II) complex $[(C(pz)_4)Ru(P(OCH_2)_3CEt)(NCMe)Me][BAr'_4]$ (pz = pyrazolyl, BAr'_4 = tetrakis[3,5-bis(trifluoromethyl)phenyl]borate) undergoes intramolecular C–H activation of a pyrazolyl ring. DFT calculations revealed that the different reactivity of $TpRu(P(OCH_2)_3CEt)(NCMe)Ph$ and $[(C(pz)_4)Ru(P(OCH_2)_3CEt)(NCMe)Me][BAr'_4]$ is a result of the stronger binding of the Tp pyrazolyl rings to Ru(II) compared to that of $C(pz)_4$.

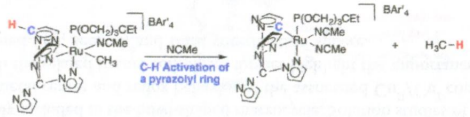

6280 dx.doi.org/10.1021/ic500824r

EXAFS Study into the Speciation of Metal Salts Dissolved in Ionic Liquids and Deep Eutectic Solvents

Jennifer M. Hartley, Chung-Man Ip, Gregory C. H. Forrest, Kuldip Singh, Stephen J. Gurman, Karl S. Ryder, Andrew P. Abbott, and Gero Frisch*

Speciation of 25 metal salts in various deep eutectic solvents and imidazolium ionic liquids has be determined during EXAFS. The solvent controls the speciation. There is no fundamental difference between ionic liquids and deep eutectic solvents.

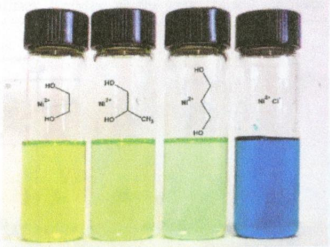

6289 Ⓢ dx.doi.org/10.1021/ic5008507

Mild Hydrothermal Crystal Growth, Structure, and Magnetic Properties of Ternary U(IV) Containing Fluorides: $LiUF_5$, KU_2F_9, $K_7U_6F_{31}$, $RbUF_5$, RbU_2F_9, and RbU_3F_{13}

Jeongho Yeon, Mark D. Smith, Joshua Tapp, Angela Möller, and Hans-Conrad zur Loye*

Several alkali U(IV) fluoride materials, $LiUF_5$, KU_2F_9, $K_7U_6F_{31}$, RbU_2F_9, $RbUF_5$, and RbU_3F_{13}, have been crystallized through a mild hydrothermal technique using the in situ reduction of U(VI) to U(IV). The materials exhibit complex crystal structures, and the U(IV) is observed in large coordination environments. The temperature dependent magnetic property measurements indicated that the U(IV) exhibits a singlet ground state at low temperatures.

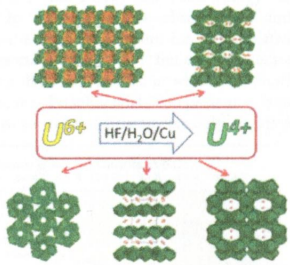

6299 Ⓢ dx.doi.org/10.1021/ic5008582

Two-Dimensional 3d–4f Heterometallic Coordination Polymers: Syntheses, Crystal Structures, and Magnetic Properties of Six New Co(II)–Ln(III) Compounds

Pau Díaz-Gallifa, Oscar Fabelo,* Jorge Pasán, Laura Cañadillas-Delgado, Francesc Lloret, Miguel Julve, and Catalina Ruiz-Pérez*

The synthesis of new 3d–4f metal-organic frameworks (MOFs) through slow diffusion techniques seems to be a suitable alternative method to prepare heterometallic systems. Herein, we present the synthesis and magneto-structural study of six new Co(II)–Ln(III) complexes, which provide the first examples of magnetic modeling on Co(II)–Ln(III) systems with the six-coordinate cobalt(II) ion in a compressed octahedral environment.

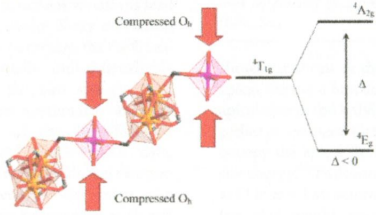

6309 dx.doi.org/10.1021/ic500862b

Characterization of the Zn(II) Binding Properties of the Human Wilms' Tumor Suppressor Protein C-terminal Zinc Finger Peptide

Ka Lam Chan, Inna Bakman, Amy R. Marts, Yuksel Batir, Terry L. Dowd, David L. Tierney, and Brian R. Gibney*

The formation constant for a natural Cys_2His_2 $\beta\beta\alpha$ zinc finger peptide has been determined using a suite of equilibrium measurements. These data are compared to literature values for Zn(II)–Cys_2His_2 protein events to assess the free energy cost of protein folding in proteins with metal-induced protein folding events. The data lead to the conclusion that the free energy contribution of Zn(II) binding is far in excess of the minimal free energy cost of protein folding.

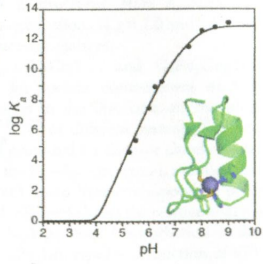

6321 dx.doi.org/10.1021/ic500938k

Changing Hafnium Speciation in Aqueous Sulfate Solutions: A High-Energy X-ray Scattering Study

Ali Kalaji, S. Skanthakumar, Mercouri G. Kanatzidis, John F. Mitchell, and L. Soderholm*

High-energy X-ray scattering and Raman spectroscopy were used to probe hafnium speciation in aqueous solutions and changes that occur with the introduction of varying concentrations of sulfate. The atomic correlations, determined from single-crystal studies of precipitates that form from these solutions, are compared and contrasted with those seen in the aqueous phase itself. The results point to the presence of multiple hafnium complexes and potential equilibria connecting them, thereby providing insights into possible crystallization mechanisms.

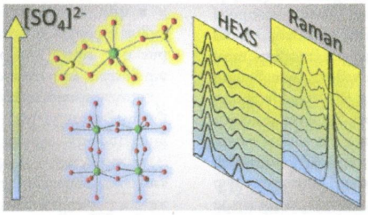

6329 dx.doi.org/10.1021/ic500910z

Modeling the Active Site of [NiFe] Hydrogenases and the [$NiFe_u$] Subsite of the C-Cluster of Carbon Monoxide Dehydrogenases: Low-Spin Iron(II) Versus High-Spin Iron(II)

Katharina Weber, Özlen F. Erdem, Eckhard Bill, Thomas Weyhermüller, and Wolfgang Lubitz*

A series of [NiFe] complexes related to both the C-cluster [$NiFe_u$] subsite of CO dehydrogenase and the active site of [NiFe] hydrogenases was synthesized and characterized. The electronic structure is assigned as Ni(II) low spin/Fe(II) high spin, similar to the reduced C state of Ni-containing CODH.

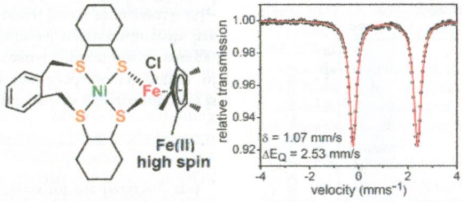

6338 dx.doi.org/10.1021/ic500969r

Synthesis and Analysis of a Family of Cerium(IV) Halide and Pseudohalide Compounds

Ursula J. Williams, Patrick J. Carroll, and Eric J. Schelter*

A series of cerium(IV) halide and pseudohalide complexes were isolated by silyl halide exchange reactions of a cerium(IV) fluoride precursor. Characterization of the cerium(IV) series showed that spectroscopic and electrochemical behavior varied with the identity of the halide or pseudohalide ligand.

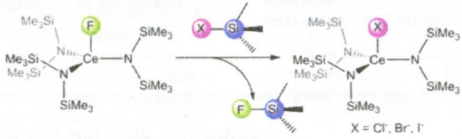

dx.doi.org/10.1021/ic500971z

Enlarging the π System of Phosphorescent (C^C*) Cyclometalated Platinum(II) NHC Complexes

Alexander Tronnier, Alexander Pöthig, Stefan Metz, Gerhard Wagenblast, Ingo Münster, and Thomas Strassner*

Six new (C^C*) cyclometalated Pt(II) NHC complexes with varying size of the π system in the ligand backbone are presented together with their solid-state structures and photophysical properties. Quantum yields as high as 81% at room temperature were measured, with emission maxima in the blue-green region of the visible spectrum.

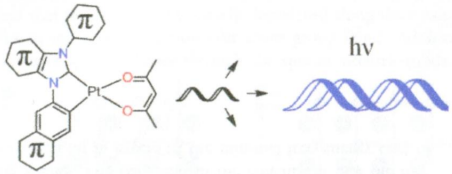

Supporting Information available via online article